mathematics

MDPI

Article

The Resilience of an Urban Rail Transit Network: An Evaluation Approach Based on a Weighted Coupled Map Lattice Model

Yuhao Wang [1], Jie Liu [1,2,*] and Zhouyu Li [1]

[1] Faculty of Transportation Engineering, Kunming University of Science and Technology, Kunming 650500, China; yuhao7195@163.com (Y.W.); lizhouyu@stu.kust.edu.cn (Z.L.)
[2] Department of Engineering, University of Cambridge, Cambridge CB2 1PZ, UK
* Correspondence: liu_jie521188@163.com

Abstract: Modeling cascading failure in an urban rail transit network (URTN) is essential for evaluating the impact of interruptions and network resilience. Here, a weighted coupled map lattice (CML) model is proposed. This model combines structural network coupling and passenger flow coupling to analyze the cascading failure process triggered by a station failure. Four network performance indicators are developed: network efficiency and subgraph connectivity from the network structure perspective, and OD connectivity and the reciprocal of average transfers from the network service perspective. The resilience of a URTN is measured based on the network performance indicators during station failures. Application of the model to the Wuhan URTN showed that station failure with high numbers of boarding and alighting passengers caused the highest decline in network resilience. The network's structural resilience was stronger than its service resilience. The relationship between the percentage of failed stations and network performance indicated a significant threshold effect at a 5% failure percentage. Specifically, network performance decreased rapidly when the percentage of failed stations was below 5% and more gradually when it exceeded this threshold. Moreover, network performance exhibited high sensitivity to increases in external perturbation intensity when the failure station percentage was below 5%, but this sensitivity diminished significantly once the percentage surpassed 5%.

Keywords: transport resilience; urban rail transit; cascading failure; coupled map lattice model

MSC: 46-02

check for updates

Academic Editor: Aleksandr Rakhmangulov

Received: 11 January 2025
Revised: 3 February 2025
Accepted: 11 February 2025
Published: 13 February 2025

Citation: Wang, Y.; Liu, J.; Li, Z. The Resilience of an Urban Rail Transit Network: An Evaluation Approach Based on a Weighted Coupled Map Lattice Model. *Mathematics* **2025**, *13*, 608. https://doi.org/10.3390/math13040608

Copyright: © 2025 by the authors. Licensee MDPI, Basel, Switzerland. This article is an open access article distributed under the terms and conditions of the Creative Commons Attribution (CC BY) license (https://creativecommons.org/licenses/by/4.0/).

1. Introduction

The urban rail transit network (URTN) is a crucial component of the urban public transport system and serves as essential infrastructure within the city [1,2]. It plays a vital role in meeting urban commuter demand and enhancing mobility in cities. The safe and stable operation of the URTN is essential for residents' daily travel and the smooth functioning of social activities. An efficiently operating URTN not only provides convenient transportation services but guarantees a safe and reliable travel experience for urban inhabitants. Therefore, the resilience of a URTN is important for maintaining its service quality during perturbance. In the 1970s, Holling [3] introduced ecology resilience, representing the stability and recovery capabilities of an ecosystem in the face of external natural and human factors. Resilience was gradually introduced into other disciplines later. In the transportation field, the resilience of a transportation network reflects the ability of the network to maintain and quickly restore a normal state under perturbance [4–6]. In

recent years, frequent disruption accidents caused by natural disasters and human factors have seriously affected the safety and efficient operation of URTN [7,8]. For example, Zhengzhou, China experienced rare torrential rain, which led to the shutdown of the URTN and resulted in 14 deaths and five injuries. Many similar incidents have highlighted the critical importance of the study of URTN resilience.

The resilience of URTNs has become a hot research topic in recent years. Researchers usually study the resilience of URTNs from the network structure perspective by applying the complex network theory. This method is simple and applicable to large-scale networks [9–12]. In such studies, researchers often adopt L-space [13,14] methods to represent transportation networks as connected graphs. In the connected graphs, the stations or road intersections are represented as nodes, and rails among stations or roads among intersections are represented as edges. Then, indicators such as the network efficiency [15,16], the average clustering coefficient [13,17], and the relative size of the largest connected subgraph [18] are used to evaluate the performance of the network. The simulation of network interruptions involves inducing failures in nodes or edges. Various recovery methods, such as the exhaustive method [19], priority recovery [20], sequential optimization model-based recovery [21], and an adaptive method based on reinforcement learning [22] have been employed to represent the network recovery process. The network's resilience is evaluated based on the decline in network performance during the network failure and recovery process.

Research has exploited the utility of topological analysis in resilience quantification but provided limited operational insights without considering the travel demand and passage behaviors. Therefore, some scholars have studied the resilience of transportation networks from the perspective of passenger travel. Adjetey et al. [23] used passenger load and passenger delay as network performance indicators to evaluate the resilience of railway networks. Voltes [24] adopted passenger flow delay within a day as an indicator and highlighted the benefits of flow and demand modeling in obtaining accurate results. Lu [25] integrated network topology and passenger volume to quantify the resilience of a rail network under incidents. Chen et al. [26] compared the topological and functional resilience of subnetworks and multimodal networks under different disruptions. Ouyang et al. [27] proposed two performance indicators, railway accessibility and flow-based vulnerability, for assessing the performance of railway networks. Cleod et al. [28] proposed an approach using shortest-path passenger flow assignment to quantify the delays experienced by passengers due to disruptive events.

Station failures inevitably lead to passenger route adjustments [29,30], resulting in passengers being transferred to stations adjacent to the failed stations [31]. When the passenger load of an adjacent station or section exceeds its capacity, this may trigger a new round of station or section failure. For this reason, some scholars have used the coupled map lattice (CML) model to describe the process of cascading failure. For instance, Feng et al. [32] represented the Shanghai URTN using L-space and P-space models, while a CML model was employed to simulate cascading failures. Ye and Luo [33] proposed an improved CML model based on graph attention networks to investigate the cascading failure process of metro networks. Sun et al. [12] employed the CML model to analyze cascading failures in the weighted Beijing URTN, considering the loading and redistribution of multistatic passenger flow. Lu et al. [34] used the CML model to study network cascading failures and analyzed the changes in network topology and functional characteristics. Shen et al. [35] proposed a bidirectional CML model to investigate cascading failures, taking into account the system's initial equilibrium state, load matching, and capacity-based load redistribution.

As outlined above, the CML model is widely used to assess transport performance because of its ability to accurately simulate the propagation of cascading failures across

networks. However, the coupling between the network structure and network passenger flow has not been fully integrated when developing the CML model to assess the resilience of URTNs. A more comprehensive evaluation of URTN resilience, considering both network structure and passenger flow perspectives under various station failure scenarios and recovery strategies, requires further investigation. Additionally, the relationship among perturbation intensity, network coupling degree, and the reduction in URTN performance has yet to be explored. To address these gaps, this paper focuses on the following work: (1) Existing studies do not consider the boarding and alighting passengers at stations when modeling the coupling strength between stations. This paper uses station degree value, passenger flow on links, and boarding and alighting passengers to measure the structure-based coupling and passenger-flow-based coupling among stations, and a weighted CML model based on the coupling measure is developed. (2) This paper proposes four indicators from both the network structure and service aspects to analyze network resilience comprehensively. Moreover, considering the limitations of traditional giant component size indicators in understanding minor subgraphs, the proposed subgraph connectivity indicator measures the size of all connected subgraphs after network failure. (3) Various failure and recovery methods were adopted to study the resilience of Wuhan URTN under different failure scenarios, which comprehensively depicted the network dynamics after different station failure. Using the proposed resilience evaluation method, the relation among perturbation intensity, network coupling degree, and the decline in URTN performance was revealed.

2. Methods

The L-space method is used to describe an URTN. The stations and sections among stations are represented with the nodes and edges, and thus an URTN is abstracted as a graph $G = (V, E)$. V and E are the set of nodes and set of edges on the graph, respectively.

2.1. Station Coupling Measures

A station's degree indicates the number of stations directly connected to it, which measures the connectivity and structure-based coupling among stations. The passenger flow on links and the boarding and alighting passengers measure the passenger-flow-based coupling among stations. This paper combines both structural and passenger-flow coupling between the stations.

2.1.1. Station Degree

The station degree refers to the number of stations directly connected to the station in the network. The greater the station degree value, the greater the impact of the station on its adjacent stations.

$$K_i = \sum_j a_{ij} \tag{1}$$

where K_i is the degree of station i and a_{ij} is the adjacency matrix. When station i is directly connected with station j, $a_{ij} = 1$, otherwise, $a_{ij} = 0$.

2.1.2. Passenger Flow on Links

The passenger flow on links is the number of passengers passing through adjacent stations, which measures the coupling intensity for adjacent stations in terms of passenger flow. A larger passenger flow on links indicates that the operational status of one station has a greater impact on its adjacent stations.

$$f_{ij} = \sum_{o \in S} \sum_{d \in S, o \neq d} V_{od} * \delta_{od}^{ij} \tag{2}$$

where f_{ij} denotes the interval passengers flow from station i to station j; V_{od} represents the number of passengers travelling from origin station o to destination station d; and δ_{od}^{ij} is a binary, where $\delta_{od}^{ij} = 1$ indicates that the passengers travelling from station o to station d pass through station i to station j, and otherwise $\delta_{od}^{ij} = 0$. δ_{od}^{ij} can be determined using the passenger assignment method.

2.1.3. Boarding and Alighting Passengers at Stations

In the event of a station malfunction, passengers may choose to board or alight at adjacent stations. The fluctuations in the volume of boarding and alighting passengers directly affect passengers at their neighboring stations. Therefore, in addition to passenger flow on links, the boarding and alighting passengers at stations are used to measure the coupling degree of stations in terms of passenger flow.

$$l_i = l_i^{in} + l_i^{out} \tag{3}$$

where l_i denotes the total boarding and alighting passengers at station i, l_i^{in} denotes the boarding passenger flow at station i, and l_i^{out} refers to the alighting passenger flow at station i.

2.2. Weighted CML Model for the URTN Based on Station Coupling Measures

2.2.1. Weighted CML Model

The CML model is widely used in the temporal and spatial dynamics of complex networks in many fields. In the field of transportation, it can be used to analyze the cascading failure process on a traffic network, where the failure of one station causes the failure of its adjacent stations in succession. This weighted CML model for a URTN is developed based on station coupling measures, which comprehensively integrate the interdependent relations and impacts among stations. Three station coupling measures, i.e., station degree, passenger flow on links, and boarding and alighting passengers at stations, are integrated into the weighted CML model from the network structure and passenger travel perspectives.

$$x_i(t+1) = \left| \begin{array}{c} (1-\varepsilon_1-\varepsilon_2-\varepsilon_3) * g(x_i(t)) + \varepsilon_1 \sum_{j=1, j\neq i}^{N} a_{ij} * \frac{g\left(x_j(t)\right)}{K_i} + \\ \varepsilon_2 \sum_{j=1, j\neq i}^{N} a_{ij} * \left(f_{ij} + f_{ji}\right) * \frac{g\left(x_j(t)\right)}{\sum\limits_{j}\left(f_{ij}+f_{ji}\right)} + \\ \varepsilon_3 \sum_{j=1, j\neq i}^{N} a_{ij} * l_j * \frac{g\left(x_j(t)\right)}{\sum\limits_{j} l_j} \end{array} \right| i = 1, 2, \ldots, N \tag{4}$$

$$g(x_i) = 4x_i(1-x_i) \tag{5}$$

where $x_i(t+1)$, $x_i(t)$, and $x_j(t)$ are the operational status of station i at time $t+1$, the operational status of station i at time t, and the operational status of station j at time t, respectively, which evaluate their service level. The initial status of a station i, $i = 1, 2, \ldots, N$, is determined by the initial passenger flow and its maximum capacity, as per Equations (6) and (7). Therefore, when $x_i(t+1) \geq 1$, station i is treated as in a failure state with a low service level; otherwise, it is functioning normally. The operational status of a station i, $i = 1, 2, \ldots, N$, represented as $x_i(t+1)$, is updated according to its status at time t, the status of its adjacent stations, and the station coupling degree. The coefficient ε_1 is the structure-based coupling coefficient, representing the intensity of station coupling measured by the station degree. ε_2 and ε_3 are the passenger-flow-based coupling coefficients, representing the intensity of station coupling measured by passenger flow on links and boarding and alighting passengers at stations, respectively. In the weighted CML

model, $\varepsilon_1, \varepsilon_2, \varepsilon_3 \in (0,1)$, and $\varepsilon_1 + \varepsilon_2 + \varepsilon_3 < 1$. l_j represents the boarding and alighting passengers of stations adjacent to station i. $g(x_i)$ is the chaotic logistic mapping function, and $g(x_i) = 4x_i(1 - x_i)$ is used to represent the evolution law of the station capacity constraint [36] when $0 \leq x_i \leq 1, 0 \leq g(x_i) \leq 1$.

$$x_i(0) = \frac{f_i(0)}{c_i}, i = 1, 2, \ldots, N \tag{6}$$

$$c_i = w_i * s_i, i = 1, 2, \ldots, N \tag{7}$$

where $x_i(0)$ and $f_i(0)$ represent the initial status of station i and its passenger flow at the initial stage, respectively. c_i is the maximum capacity of station i, determined by the capacity of a train passing station w_i and the number of trains passing station s_i.

2.2.2. Perturbance and Cascading Failure Simulation

To simulate the perturbance at any station $i, i = 1, 2, \ldots, N$, at a time t, the operational status of a station x_i can be set as $x_i(t+1) + R$. $R, R > 1$ is a random parameter that qualitatively characterizes the magnitude of perturbance. A larger R indicates a greater-intensity perturbance that has a more significant impact on adjacent stations, resulting in more severe cascading failures. In the following steps, the cascading failure process of the network is determined by updating the station operation status with the weighted CML model, and failed stations, for which the operational status values exceed 1, can be identified.

2.3. Network Resilience Indicators

In network resilience research, transportation networks' resilience is typically evaluated using cumulative performance loss during interference periods. As depicted in Figure 1, when the perturbance occurs at time t_0, the URTN performance keeps decreasing to the lowest point at time t_1. Then, the network gradually recovers because of implemented recovery measures until it reaches normal operational status at time t_2. $Q(t)$ represents the performance indicator value of the network at time t. q_0 and q_1 denote the performance indicator values of the network at times t_0 and t_1, respectively.

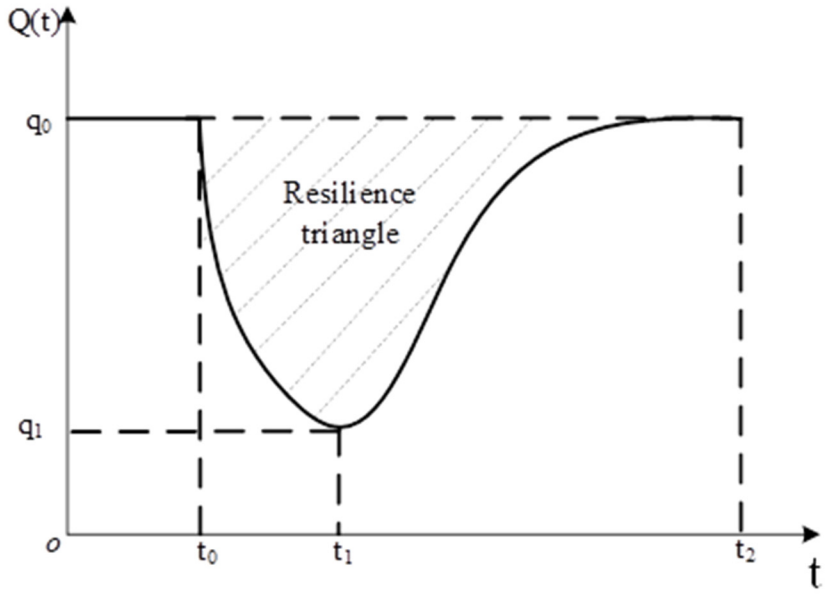


Figure 1. Resilience triangle diagram.

In this paper, the network's resilience is evaluated based on the decline in network performance during the network failure and recovery process. To assess the network performance, several indicators are proposed, including network efficiency, subgraph connectivity, OD connectivity, and the reciprocal of average transfers. During the failure and recovery processes, the cumulative reduction of each indicator is utilized to measure the resilience.

2.3.1. Network Structure Performance

During the perturbance, the shortest paths on the network are subject to alteration, resulting in an increase in the average shortest path length. The network efficiency indicator reflects the transportation efficiency of the network from a structure perspective.

$$P_1(t) = \frac{1}{N(N-1)} \sum_{i=1}^{N} \sum_{j=1, j \neq i}^{N} \frac{1}{d_{ij}(t)} \tag{8}$$

where $P_1(t)$ represents the network efficiency of the URTN at time t, N represents the total number of stations, and $d_{ij}(t)$ represents the shortest path length from stations i to j.

The traditional largest connected subgraph indicator focuses solely on the largest connected subgraph on the network, neglecting the impact of other, smaller subgraphs on the network's overall connectivity. To address this limitation, an indicator considering the connectivity of all subgraphs on the network is proposed.

$$P_2(t) = \sum_{m=1}^{M} \frac{N_m}{N - \sum_{h=1}^{m} N_{h-1}} * \frac{N_m}{N}, m = 1, 2 \ldots M \tag{9}$$

where $P_2(t)$ denotes the subgraph connectivity of the URTN at time t; N_m is the number of stations in the m-th connected subgraph, where N_m is arranged in descending order by the number of stations and $N_0 = 0$; M denotes the total number of all connected subgraphs; $\frac{N_m}{N - \sum_{h=1}^{m} N_{h-1}}$ denotes the proportion of stations in the m-th connected subgraph relative to the total stations remaining in the network after excluding bigger connected subgraphs; and $\frac{N_m}{N}$ indicates the proportion of stations in the m-th connected subgraph relative to the total number of stations, reflecting the weighting of this subgraph in the calculation.

2.3.2. Network Service Performance

During the network perturbance, the path among some OD pairs may be disrupted, which renders rail transit unusable for passengers travelling among those ODs. Therefore, the number of passengers able to utilize rail transit is taken as an indicator for evaluating the network service performance.

$$P_3(t) = \frac{\sum_{i=1}^{N} \sum_{j=1, j \neq i}^{N} \delta_{ij}(t) * v_{ij}(t)}{\sum_{i=1}^{N} \sum_{j=1, j \neq i}^{N} v_{ij}(t)} \tag{10}$$

where $P_3(t)$ denotes the OD connectivity of the URTN at time t and $v_{ij}(t)$ denotes the number of passengers travelling from station i to j at time t. When $\delta_{ij}(t) = 1$, there exists a connected rail transit path from station i to j, enabling passengers to utilize rail transit. Conversely, when $\delta_{ij}(t) = 0$, there is no connected path from station i to j, and passengers are unable to utilize rail transit.

Station failures may also prompt passengers to resort to detour routes, increasing the number of transfers. Even when travelling on the same line, passengers may need to alight and reboard another train when trains run short routes on the line. To reflect this situation,

we use paired boarding and alighting times as the transfer count. The reciprocal of average transfers per passenger is utilized to reflect network service performance.

$$P_4(t) = \frac{\sum_{i=1}^{N}\sum_{j=1,j\neq i}^{N}\frac{1}{0.5*h_{ij}(t)}*v_{ij}(t)}{\sum_{i=1}^{N}\sum_{j=1,j\neq i}^{N}v_{ij}(t)} \tag{11}$$

where $P_4(t)$ represents the reciprocal of average transfers per passenger on the URTN at time t and $h_{ij}(t)$ represents the number of boarding and alighting times along the route from station i to station j. The paired boarding and alighting times are used to count the number of transfers, and thus, $h_{ij}(t)$ is multiplied by 0.5.

2.4. Network Resilience Assessment

Network resilience is evaluated based on the cumulative loss of network performance.

$$R_k = \int_{t_{start}}^{t_{end}}\left[P_k^0(t) - P_k(t)\right]dt; \mathrm{k} = 1,2,3,4 \tag{12}$$

where R_k represents the assessment result of network resilience based on the k-th network performance indicator (where $\mathrm{k} = 1,2,3,4$ correspond to the network resilience using network efficiency, subgraph connectivity, OD connectivity, and reciprocal of average transfers per passenger, respectively, as network performance indicators). $P_k^0(t)$ denotes the k-th network performance indicator under normal network operation at time t. $P_k(t)$ is computed according to Equations (8)–(11). t_{start} and t_{end} denote the start time of the perturbance and the time when the network returns to normal operation, respectively.

The steps for measuring the resilience of a URTN based on this weighted CML model are illustrated in Table 1.

Table 1. Steps for measuring URTN resilience.

Step	**1**	Initialize the value of ε, the value of the intensity perturbance R, and the percentages of failed stations; Calculate the initial status of all stations $x_i(0) = \frac{f_i}{c_i}$; $g(x_i) = 4x_i(1-x_i)$.
Step	**2:**	Cascade failure propagation: **For** (each station in the failed stations): Store their adjacent stations; Calculate the status of adjacent stations $x_i(t)$ at time t; Remove the failed stations from the network; **End**
Step	**3:**	Calculate the performance of the network at time t, $P_k(t)$ $(k = 1,2,3,4)$.
Step	**4:**	Identify new failed stations: **For** (each station in the adjacent stations): **if** $x_i(t) > 1$: Store the adjacent stations as new failed stations; **End** **End**
Step	**5:**	Return to step 2 until there are no new failed stations.
Step	**6:**	Calculate the resilience of the network, R_k $(k = 1,2,3,4)$.

3. Results

Wuhan, situated in central China, holds prominence as one of the largest cities in China, populated by over 13 million people. By April 2019, the Wuhan URTN had expanded to encompass nine operational lines and 190 stations, collectively spanning 319.87

km. Notably, the system accommodates an average daily ridership nearing 3 million passengers, constituting approximately 40% of Wuhan's total public transportation users. This extensive subway infrastructure significantly contributes to the amelioration of urban traffic congestion within the city. The layout of the Wuhan URTN in April 2019 is shown as Figure 2.



Figure 2. Wuhan URTN layout in April 2019.

3.1. The Resilience of the Network Under Different Failures

Three commonly used failure modes were employed to analyze the network's resilience to different failures. These three failure modes involved simulating station failure according to degree-based sequencing, link-flow-based sequencing, and boarding and alighting passenger sequencing. During the network recovery stage, the failed stations' recovery sequence was determined the same way. To analyze the network resilience to a certain fraction of station failures with three failure modes, 2.5% of stations on the network failed with these three failure modes. The values of ε_1, ε_2, and ε_3 in the weighted CML model were set to 0.25, and the perturbation intensity R was set to 2. During the station failure and recovery process, the failure or recovery for each station was assumed to take one unit of simulation time (one time step). The network cascading failure process was integrated during the simulation, and the network performance was computed during each simulation time step. The changes in network performance during simulation were recorded and are depicted graphically in Figure 3, and the cascading failure diffusion results are shown in Figure 4.

The resilience loss values of the network were calculated based on Equation (12). The network resilience loss during the perturbance is shown in Table 2. Figure 3 and Table 2 show that the station failure mode with boarding and alighting passenger sequencing caused a high decrease in network resilience. Among the different station failure modes, the station failure mode with link-flow-based sequencing had the lowest impact on the network's resilience.

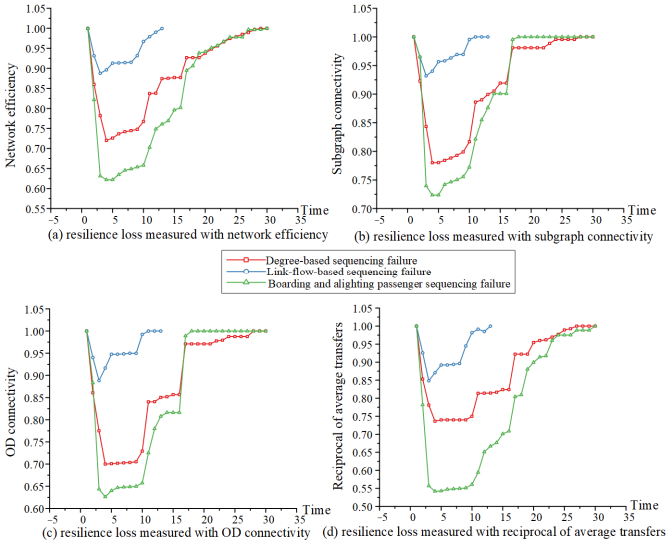


Figure 3. Network performance change in the three failure modes.

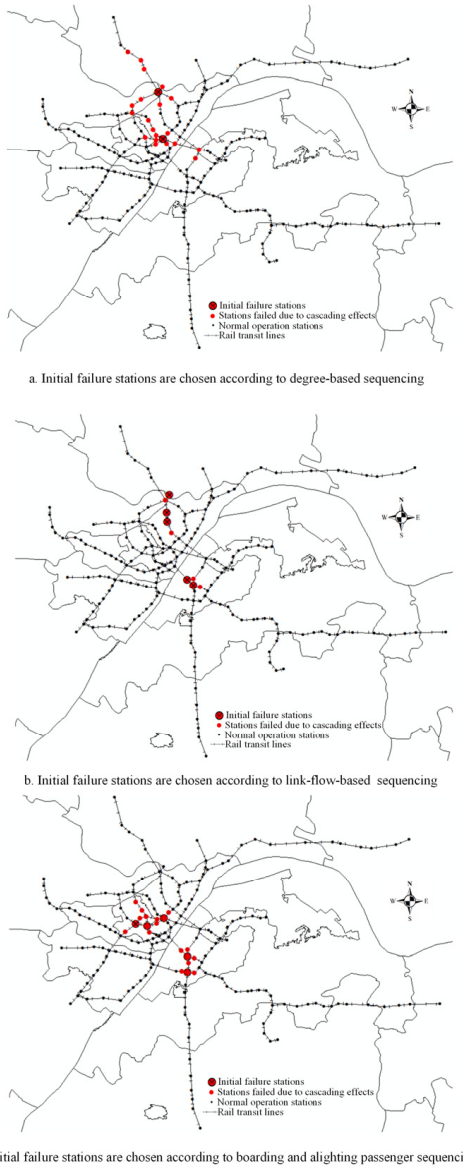


Figure 4. Cascading failure result for three failure modes.

Table 2. Resilience loss values in the three failure modes.

Failure Modes Loss of Resilience	Degree-Based Sequencing	Link-Flow-Based Sequencing	Boarding and Alighting Passenger Sequencing
Network efficiency	3.48	0.76	5.00
Subgraph connectivity	2.42	0.35	2.83
OD connectivity	3.57	0.52	4.21
Reciprocal of average transfers	3.92	0.87	6.74

To reveal the resilience of the Wuhan URTN when different fractions of stations failed with three modes, the network resilience losses corresponding to different fractions of station failure were computed and are shown in Figure 5. Figure 5 shows that among the three failure modes, the station failure mode with boarding and alighting passenger sequencing exhibited the most significant reduction in network resilience. Conversely, the station failure mode with link-flow-based sequencing demonstrated the least impact on network resilience, whereas the station failure mode with degree-based sequencing resulted in resilience reductions intermediate to the other two modes. The reason for this was that the stations selected with link-flow-based sequencing were adjacent, which tended to result in localized cascade failures. Conversely, the failed stations selected by boarding and alighting passenger sequencing and degree-based sequencing were typically distributed across the network, potentially initiating extensive cascading failures throughout the network. The cascade diffusion in Figure 4 confirms this point.

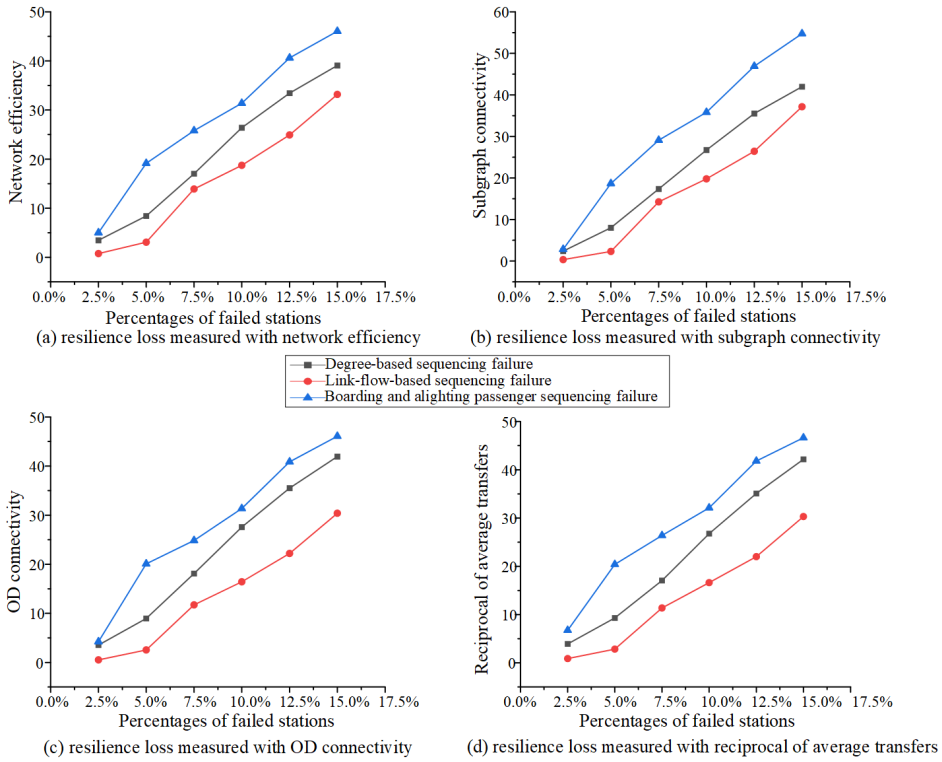


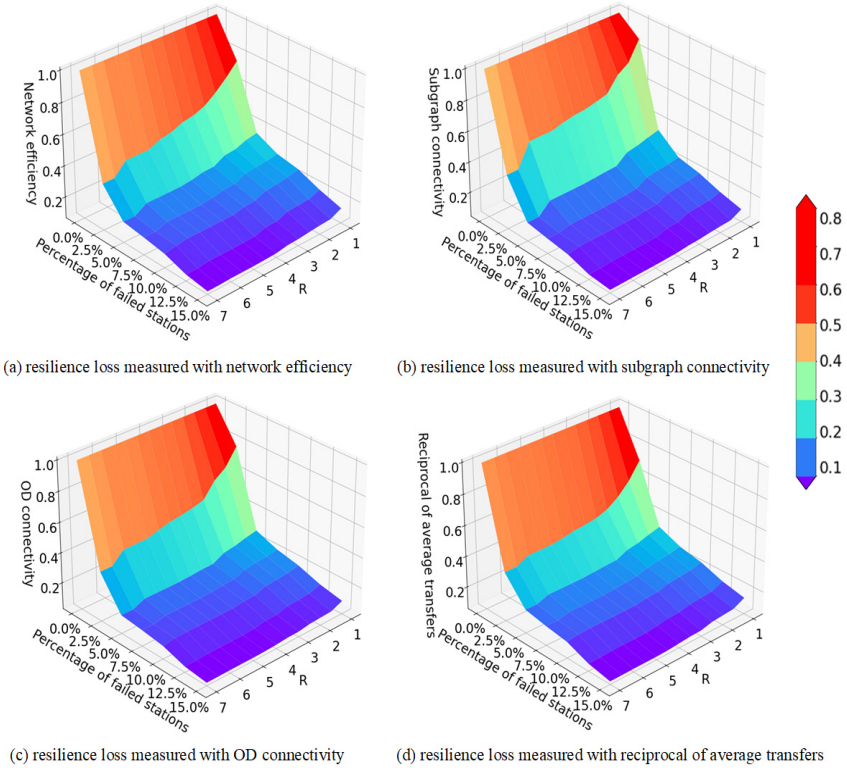
Figure 5. Resilience loss values at different percentages of failed stations.

Among the four performance indicators, the reciprocal of average transfers decreased most significantly, whereas the subgraph connectivity indicator based on structure performance exhibited the least decline. The intermediate indicators included the network efficiency indicator and OD connectivity indicator. These findings indicate that the structural resilience of the network is higher than the service resilience. This observation can be

attributed to the strong connectivity among stations in the Wuhan URTN, which contributes to its robust structural stability. However, the passenger flow of the Wuhan URTN is high, especially on Lines 1 and 2. When a station fails in the network, it greatly affects passengers' travel and leads to a significant decline in the network service performance.

3.2. Impacts of Perturbation Intensity and Percentages of Failed Stations on Network Performance

The network recovery proceeds sequentially according to the sequence of failed stations. Identifying the stations affected by cascading failures helps determine the magnitude of network resilience loss. For analytical simplicity, subsequent sections concentrate exclusively on the final result following cascading failures. Specifically, the analysis focuses on the lowest network performance for station failures, without delving into the complexity of the network recovery process. Section 3.1 reveals that network resilience deteriorated most significantly when stations failed with boarding and alighting passengers sequencing. Therefore, in this simulation, station failure was based on the sequencing of boarding and alighting passengers. The relations among network performance, percentage of failed stations and intensity perturbance R are shown in Figure 6.



(a) resilience loss measured with network efficiency

(b) resilience loss measured with subgraph connectivity

(c) resilience loss measured with OD connectivity

(d) resilience loss measured with reciprocal of average transfers

Figure 6. The changes in network performance under different R and percentages of failed stations.

Figure 6 illustrates that under a fixed perturbance intensity R, an increasing number of failed stations correlated with a decline in network performance. Of particular note is that when the proportion of failed stations was below 5%, network performance deteriorated more rapidly. When the percentage of failed stations exceeded 5%, the performance decline notably decelerated. Therefore, under constant perturbance intensity R, the percentage threshold value of failed stations is estimated to be around 5%. This threshold effect primarily arises from the cascading failure propagation. This means that if the percentage of failed stations exceeds 5%, this could potentially lead to widespread network collapse. Consequently, maintaining the proportion of failed stations below 5% when intensity perturbance R is fixed can effectively mitigate the extent of cascading failures and prevent significant declines in network performance.

When the proportion of failed stations remained constant, with increasing perturbance intensity R, the network performance showed a declining trend. Moreover, as R increased, the decline in network performance accelerated. In addition, the slope of the linear relationship was low, which became evident when the percentage of failed stations exceeded 5%. Thus, it is effective to control cascading failure by reducing the perturbance intensity R when the percentage of failed stations is lower than 5%. However, it is difficult to prevent large-scale paralysis of the network by mitigating the perturbance intensity R when the percentage of failed stations is high.

3.3. Parameter Sensitivity Analysis

The coupling strength between stations signifies the degree of correlation between them and is determined by the coupling coefficient. A higher coupling coefficient indicates a more tightly interconnected relationship and intensifies cascading failure propagation. Therefore, it is crucial to investigate how different coupling coefficients affect the cascading failure propagation within networks.

Here, the structure-based coupling coefficient ε_1 on network performance was investigated from the perspective of network structure, and the station failure mode was degree-based sequencing. The value of ε_1 ranged from 0 to 0.8, with intervals of 0.1, in the sensitivity analysis. The passenger-flow-based coupling coefficients ε_2 and ε_3 were adjusted in relation to the structural coupling coefficient ε_1, following the relationships defined in Equations (13) and (14) for the weighted CML model. Analyzing the variations in ε_1 on network performance also reflects the changes in ε_2 and ε_3. Therefore, the relation between network passenger-flow-based coupling and network performance after station failure can also be analyzed according to the relation between network structure-based coupling and network performance. The conclusions drawn from these two relationships are precisely opposite.

$$\varepsilon_1 + \varepsilon_2 + \varepsilon_3 = 0.8 \tag{13}$$

$$\varepsilon_2 = \varepsilon_3 \tag{14}$$

Based on Figure 7, as the structure-based coupling coefficient ε_1 increased, the network performance measured by the four indicators displayed a similar trend. This occurred primarily because different coupling coefficients directly result in varying numbers of failure stations. However, these indicators are calculated using the same failure scenario, meaning that the failure stations are the same when calculated. Additionally, when 2.5% of stations in the network failed, the four indicators showed little variation with changes in the structure-based coupling coefficient ε_1. As the proportion of failed stations increased to 5% and 7.5%, higher values of ε_1 accelerated the spread of cascading failures throughout the network, resulting in a high network performance decrease. Beyond a 7.5% failure rate, the four indicators demonstrated minimal responsiveness to variations in ε_1.

Based on the results of sensitivity analysis in the URTN, several conclusions can be drawn. When there were few failed stations, the influence of the structure-based coupling coefficient ε_1 had no significant effect on network performance. This insignificance stemmed from the limited number of stations affected, where variations in ε_1 alone did not significantly alter the propagation dynamics of cascading failures. As the number of failed stations increased moderately, the structure-based coupling coefficient ε_1 began to have a noticeable impact on network performance. This effect may have arisen because the simulation simulated the failure mode with degree-based sequencing. With increases in the coupling coefficient ε_1, the failure of a station affects its adjacent stations to a greater extent, thus accelerating the spread of faults in the URTN. However, as the number of failed stations reached a high level, the influence of ε_1 diminished again. This reduction was

primarily due to widespread station failures across the network, leading to its near-total incapacitation. Consequently, variations in the structure-based coupling coefficient ε_1 resulted in only marginal fluctuations in observed performance indicators.

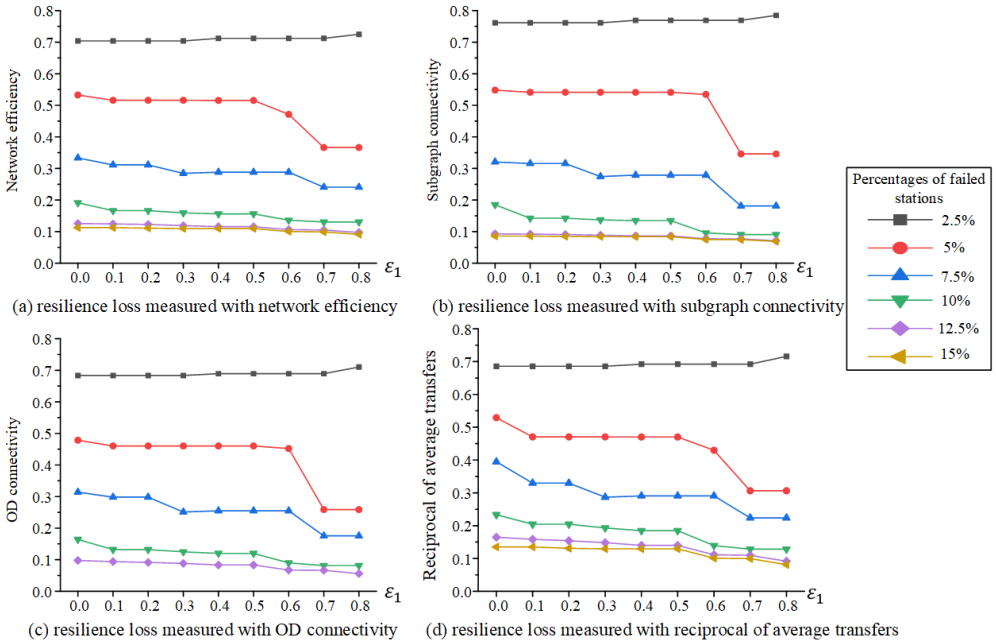


Figure 7. Sensitivity analysis of the structure-based coupling coefficient ε_1.

4. Discussion

This study delved into the resilience of the Wuhan urban rail transit network (URTN) under three failure modes. It explored the relationships among network performance, perturbation intensity, and the percentage of failed stations, with a parameter sensitivity analysis focusing on the structure-based coupling coefficient and its impact on network performance.

Existing models have limitations in integrating the coupling between network structure and passenger flow. Notably, our model overcomes this limitation and proposes four network performance indicators: network efficiency, subgraph connectivity, OD connectivity, and the reciprocal of average transfers. These four indicators establish a more comprehensive evaluation framework for network resilience. Subgraph connectivity, in particular, overcomes the limitations of traditional largest connected subgraph indicators by considering all subgraphs' connectivity.

The study's findings have significant implications for urban rail transit network operation and management. Stations with high numbers of boarding and alighting passengers, when failed, cause the most significant decline in network resilience. Urban transportation management departments are recommended to assign the highest priority to these key stations. This can be achieved by implementing more frequent maintenance schedules, installing backup power systems, and deploying additional staff during peak hours. The continuous monitoring of stations located in city centers or in the vicinity of major commercial and residential areas is also crucial, as it has the potential to significantly enhance the overall resilience of the network.

Understanding the threshold effect of failed stations (5% is a critical threshold) and perturbation intensity is crucial for emergency response strategies. When the proportion of failed stations approaches 5%, the network is at high risk. Operators should act promptly to limit the number of affected stations. As perturbation intensity in-

creases, network performance deteriorates faster, so emergency responses should focus on mitigating intensification.

However, this study has some limitations. It assumes passengers transfer only within the urban rail transit system after a station failure, while in reality, many may switch to other transportation modes. Future research should consider passenger mode-shift behaviors by developing more comprehensive models. It should also explore strategies to enhance network resilience, such as identifying and strengthening critical stations and optimizing network operations under normal and disrupted conditions. Additionally, the weighted CML model and resilience evaluation method need further validation in different urban rail transit networks to assess their generalizability and applicability. Furthermore, when applying them to analyze other networks, three data sets are required: a network graph representing the adjacency relations of links and stations, OD passenger demand for the network, and capacities of stations and links. These data are fundamental for the model to evaluate the performance of different URTNs.

5. Conclusions

This paper proposes a weighted CML model to simulate the cascading failure process in the URTN and introduces a resilience evaluation method based on the weighted CML model. The model integrates both structure-based and passenger-flow-based couplings between stations. Additionally, comprehensive network performance indicators, from both structural and service perspectives, are proposed to assess the resilience of the network.

A real-world case study of the Wuhan URTN was conducted, leading to the following conclusions based on the evaluation results. Firstly, among the three failure and recovery modes, sequencing based on boarding and alighting passenger volumes led to the most significant decline in network resilience. Therefore, ensuring the normal operation of stations with high boarding and alighting volumes is crucial to avoiding a rapid decline in network performance. Secondly, the percentage of failed stations exhibited a strong threshold effect on network performance, with the threshold being approximately 5%. Thus, in the event of perturbations, the percentage of affected stations in the Wuhan URTN should be kept below 5%. Additionally, perturbation intensity had a substantial influence on network performance, as an increase in perturbation intensity R accelerated the decline in network performance. Hence, timely mitigation of perturbance intensification is critical to preserving network service. Thirdly, in the degree-based failure and recovery mode, the structure-based coupling coefficient had minimal impact on network resilience when there were either too many or too few failed stations. However, when the number of failed stations was moderate, an increase in the structure-based coupling coefficient led to a decrease in network resilience, while the passenger-flow-based coupling coefficient had the opposite effect.

This study has several limitations. First, it assumes that after a station fails, passengers can transfer to adjacent stations and continue using the urban rail transit system. In reality, some passengers may switch to other modes of transportation, so future research should consider the impact of these mode shifts. Second, while this paper proposes a method for measuring the resilience of the URTN, it does not explore strategies for enhancing resilience, which is important for improving the URTN's capacity to respond to perturbance.

Author Contributions: The authors confirm contributions to the paper as follows. Study conception and design: J.L. and Y.W.; data collection: J.L.; analysis and interpretation of results: J.L. and Y.W.; draft manuscript preparation: Z.L. and Y.W. All authors have read and agreed to the published version of the manuscript.

Funding: The authors thank the General Project of Basic Research Program of Yunnan Province (202401AT070382, 202301AU070052), Kunming University of Science and Technology (KUST—xk2022002).

Data Availability Statement: The original contributions presented in this study are included in the article. Further inquiries can be directed to the corresponding author.

Conflicts of Interest: The authors declare that they have no known competing financial interests or personal relationships that could have appeared to influence the work reported in this paper.

References

1. Hayes, S.; Desha, C.; Burke, M.; Gibbs, M.; Chester, M. Leveraging socio-ecological resilience theory to build climate resilience in transport infrastructure. *Transp. Rev.* **2019**, *39*, 677–699. [CrossRef]
2. Wei, Y.; Yang, X.; Xiao, X.; Ma, Z.; Zhu, T.; Dou, F.; Wu, J.; Chen, A.; Gao, Z. Understanding the Resilience of Urban Rail Transit: Concepts, Reviews and Trends. *Engineering* **2024**, *41*, 7–18. [CrossRef]
3. Holling, C.S. Resilience and stability of ecological systems. *Annu. Rev. Ecol. Syst.* **1973**, *4*, 460–482. [CrossRef]
4. Freckleton, D.; Heaslip, K.; Louisell, W.; Collura, J. Evaluation of resiliency of transportation networks after disasters. *Transp. Res. Rec.* **2012**, *2284*, 109–116. [CrossRef]
5. Bababeik, M.; Khademi, N.; Chen, A. Increasing the resilience level of a vulnerable rail network: The strategy of location and allocation of emergency relief trains. *Transp. Res. Part E Logist. Transp. Rev.* **2018**, *119*, 110–128. [CrossRef]
6. Bešinović, N. Resilience in railway transport systems: A literature review and research agenda. *Transp. Rev.* **2020**, *40*, 457–478. [CrossRef]
7. Ortega, F.A.; Pozo, M.A.; Puerto, J. On-line timetable rescheduling in a transit line. *Transp. Sci.* **2018**, *52*, 1106–1121. [CrossRef]
8. Yin, J.; Ren, X.; Su, S.; Yan, F.; Tao, T. Resilience-oriented train rescheduling optimization in railway networks: A mixed integer programming approach. *IEEE Trans. Intell. Transp. Syst.* **2023**, *24*, 4948–4961. [CrossRef]
9. Jenelius, E.; Petersen, T.; Mattsson, L.-G. Importance and exposure in road network vulnerability analysis. *Transp. Res. Part A Policy Pract.* **2006**, *40*, 537–560. [CrossRef]
10. Zhang, J.; Hu, F.; Wang, S.; Dai, Y.; Wang, Y. Structural vulnerability and intervention of high speed railway networks. *Phys. A Stat. Mech. Its Appl.* **2016**, *462*, 743–751. [CrossRef]
11. Li, J.; Teng, J.; Wang, H. Measuring robustness in uncertain topologies: A study of on-demand bus networks. *Transp. A Transp. Sci.* **2024**, 1–27. [CrossRef]
12. Sun, L.; Huang, Y.; Chen, Y.; Yao, L. Vulnerability assessment of urban rail transit based on multi-static weighted method in Beijing, China. *Transp. Res. Part A Policy Pract.* **2018**, *108*, 12–24. [CrossRef]
13. Zhang, L.; Xu, M.; Wang, S. Quantifying bus route service disruptions under interdependent cascading failures of a multimodal public transit system based on an improved coupled map lattice model. *Reliab. Eng. Syst. Saf.* **2023**, *235*, 109250. [CrossRef]
14. Meng, Y.; Tian, X.; Li, Z.; Zhou, W.; Zhou, Z.; Zhong, M. Comparison analysis on complex topological network models of urban rail transit: A case study of Shenzhen Metro in China. *Phys. A Stat. Mech. Its Appl.* **2020**, *559*, 125031. [CrossRef]
15. Derrible, S.; Kennedy, C. The complexity and robustness of metro networks. *Phys. A Stat. Mech. Its Appl.* **2010**, *389*, 3678–3691. [CrossRef]
16. Zhang, J.; Xu, X.; Hong, L.; Wang, S.; Fei, Q. Networked analysis of the Shanghai subway network, in China. *Phys. A Stat. Mech. Its Appl.* **2011**, *390*, 4562–4570. [CrossRef]
17. Zhang, X.; Miller-Hooks, E.; Denny, K. Assessing the role of network topology in transportation network resilience. *J. Transp. Geogr.* **2015**, *46*, 35–45. [CrossRef]
18. Dunn, S.; Wilkinson, S.M. Increasing the resilience of air traffic networks using a network graph theory approach. *Transp. Res. Part E Logist. Transp. Rev.* **2016**, *90*, 39–50. [CrossRef]
19. Albert, R.; Barabási, A.-L. Statistical mechanics of complex networks. *Rev. Mod. Phys.* **2002**, *74*, 47. [CrossRef]
20. Yadav, N.; Chatterjee, S.; Ganguly, A.R. Resilience of urban transport network-of-networks under intense flood hazards exacerbated by targeted attacks. *Sci. Rep.* **2020**, *10*, 10350. [CrossRef]
21. Martello, M.V.; Whittle, A.J.; Keenan, J.M.; Salvucci, F.P. Evaluation of climate change resilience for Boston's rail rapid transit network. *Transp. Res. Part D Transp. Environ.* **2021**, *97*, 102908. [CrossRef]
22. Sun, J.; Zhang, Z. A post-disaster resource allocation framework for improving resilience of interdependent infrastructure networks. *Transp. Res. Part D Transp. Environ.* **2020**, *85*, 102455. [CrossRef]
23. Adjetey-Bahun, K.; Birregah, B.; Châtelet, E.; Planchet, J.-L. A model to quantify the resilience of mass railway transportation systems. *Reliab. Eng. Syst. Saf.* **2016**, *153*, 1–14. [CrossRef]
24. Voltes-Dorta, A.; Rodríguez-Déniz, H.; Suau-Sanchez, P. Vulnerability of the European air transport network to major airport closures from the perspective of passenger delays: Ranking the most critical airports. *Transp. Res. Part A Policy Pract.* **2017**, *96*, 119–145. [CrossRef]

25. Lu, Q.-C. Modeling network resilience of rail transit under operational incidents. *Transp. Res. Part A Policy Pract.* **2018**, *117*, 227–237. [CrossRef]
26. Chen, X.; Ma, S.; Chen, L.; Yang, L. Resilience measurement and analysis of intercity public transportation network. *Transp. Res. Part D Transp. Environ.* **2024**, *131*, 104202. [CrossRef]
27. Ouyang, M.; Zhao, L.; Hong, L.; Pan, Z. Comparisons of complex network based models and real train flow model to analyze Chinese railway vulnerability. *Reliab. Eng. Syst. Saf.* **2014**, *123*, 38–46. [CrossRef]
28. M'cleod, L.; Vecsler, R.; Shi, Y.; Levitskaya, E.; Kulkarni, S.; Malinchik, S.; Sobolevsky, S. Vulnerability of transportation networks: The New York city subway system under simultaneous disruptive events. *Procedia Comput. Sci.* **2017**, *119*, 42–50. [CrossRef]
29. Wang, Y.; Zhao, O.; Zhang, L. Modeling urban rail transit system resilience under natural disasters: A two-layer network framework based on link flow. *Reliab. Eng. Syst. Saf.* **2024**, *241*, 109619. [CrossRef]
30. Motter, A.E.; Lai, Y.-C. Cascade-based attacks on complex networks. *Phys. Rev. E* **2002**, *66*, 065102. [CrossRef]
31. Ma, Z.; Yang, X.; Wu, J.; Chen, A.; Wei, Y.; Gao, Z. Measuring the resilience of an urban rail transit network: A multi-dimensional evaluation model. *Transp. Policy* **2022**, *129*, 38–50. [CrossRef]
32. Feng, S.; Wang, S.; Zhao, H. Cascading Failure Analysis of Urban Rail Transit Network Based on Coupled Map Lattice Model. *CICTP* **2020**, *2020*, 2074–2084. [CrossRef]
33. Ye, H.; Luo, X. Cascading failure analysis on shanghai metro networks: An improved coupled map lattices model based on graph attention networks. *Int. J. Environ. Res. Public Health* **2021**, *19*, 204. [CrossRef] [PubMed]
34. Lu, Q.-C.; Zhang, L.; Xu, P.-C.; Cui, X.; Li, J. Modeling network vulnerability of urban rail transit under cascading failures: A Coupled Map Lattices approach. *Reliab. Eng. Syst. Saf.* **2022**, *221*, 108320. [CrossRef]
35. Shen, Y.; Ren, G.; Ran, B. Cascading failure analysis and robustness optimization of metro networks based on coupled map lattices: A case study of Nanjing, China. *Transportation* **2021**, *48*, 537–553. [CrossRef]
36. Zhang, J.; Wang, Z.; Wang, S.; Shao, W.; Zhao, X.; Liu, W. Vulnerability assessments of weighted urban rail transit networks with integrated coupled map lattices. *Reliab. Eng. Syst. Saf.* **2021**, *214*, 107707. [CrossRef]

Disclaimer/Publisher's Note: The statements, opinions and data contained in all publications are solely those of the individual author(s) and contributor(s) and not of MDPI and/or the editor(s). MDPI and/or the editor(s) disclaim responsibility for any injury to people or property resulting from any ideas, methods, instructions or products referred to in the content.